Assessing the Expansion of Ground-Motion Sensing Capability in Smart Cities via Internet Fiber-Optic Infrastructure

Scott Anderson[*1], Erin Cunningham[2], Paul Barford[1], Dante Fratta[1], Tarje Nissen-Meyer[3,4], and Herb Wang[1]

Abstract

Monitoring ground motion in smart cities can improve the public safety by providing critical insights on natural and anthropogenic hazards, for example, earthquakes, landslides, explosions, infrastructure failures, and so forth. Although seismic activity is typically measured using dedicated point sensors (e.g., geophones and accelerometers), techniques such as distributed acoustic sensing have demonstrated the utility of using fiber-optic cable to detect seismic activity over comparable distances. In this article, we present the results of a study that quantifies the expansion in an area monitored for low-amplitude ground-motion events by augmenting existing point sensors with the internet fiber-optic cable infrastructure. We begin by describing our methodology, which utilizes geospatial data on point sensors and internet optical fiber deployed in metropolitan statistical areas (MSAs) in the United States. We extend these data to identify the area that can be monitored by (1) considering the observed seismic noise data in target locations, (2) applying the model from Wilson *et al.* (2021) to understand the potential coverage area gains using optical fiber sensing, and (3) optimizing the selection of fiber segments to maximize coverage and minimize deployment costs. We implement our methodology in ArcGIS to assess the additional area that can be monitored for low-amplitude ground-motion events (i.e., magnitude > 0.5) by utilizing internet fiber-optic cables in the 100 most populous MSAs in the United States. We find that the addition of internet fiber-based sensors in MSAs would increase the area monitored on average by over an order of magnitude from 1% to 12%, if the subset of fiber cable segments that maximize coverage and minimize deployment costs is chosen even if only 20% of all fibers are used.

Cite this article as Anderson, S., E. Cunningham, P. Barford, D. Fratta, T. Nissen-Meyer, and H. Wang (2024). Assessing the Expansion of Ground-Motion Sensing Capability in Smart Cities via Internet Fiber-Optic Infrastructure, *Seismol. Res. Lett.* **XX**, 1–19, doi: 10.1785/0220240049.

Introduction

Large-scale monitoring of ground motion has many applications in smart cities (For this research, we define a smart city as a city that leverages the collection, processing, analysis, and use of data from distributed sensors placed throughout the urban infrastructure to enable effective city governance and function in diverse areas of public interest, for example, mobility, economy, and facilities management, Kirimtat *et al.*, 2020.), including public safety (e.g., Dietel, 1995), transportation (e.g., Diaz *et al.*, 2020), sporting events (e.g., Vidale, 2011), industrial
1 activity, and weather (e.g., Shen *et al.*, 2021). To monitor ground motion, individual sensors are typically placed in target locations to measure phenomena of interest such as earthquakes or infrastructure movement. These sensors are selected to monitor specific amplitudes and frequency ranges of ground motion. Two of the most important considerations in sensor selection are sensitivity and cost. A high-end permanent broadband seismic station for which the low-frequency sensitivity extends to less than 0.01 Hz can cost upward of $16,000 reported in Krokidis *et al.* (2022). In addition, each sensor must include security, power, communications infrastructure to relay data streams back to a central facility, as well as computing infrastructure for data processing, analysis, and storage. An inherent limitation of these sensors is the area over which they can effectively detect motion, which is determined by

1. University of Wisconsin, Madison, Wisconsin, U.S.A., https://orcid.org/0000-0001-7785-3296 (SA); https://orcid.org/0000-0001-7874-1819 (PB); https://orcid.org/0000-0003-0478-6760 (DF); https://orcid.org/0000-0002-1631-4608 (HW); 2. Oak Ridge National Laboratory, Oak Ridge, Tennessee, U.S.A., https://orcid.org/0000-0002-9680-6812 (EC); 3. University of Oxford, Oxford, Oxfordshire, United Kingdom; 4. University of Exeter, Exeter, United Kingdom

*Corresponding author: standerson4@wisc.edu

various factors including their sensitivity and background noise in the location of their deployment.

Scientists and governments have deployed the networks of ground-motion sensors worldwide to monitor seismic activity. These networks of sensors are densely deployed in areas of active tectonic movement. Conversely, commercial organizations deploy networks of sensors for activities such as oil and natural gas exploration, to monitor mining activities, or to monitor the stability of structures after earthquakes. Deployments of these networks of sensors are in targeted loca-
2 tions, typically not in metropolitan areas. Although the data from scientific and government-sponsored seismic networks are often publicly available, the data from commercial seismic networks are private. Thus, existing networks of ground-motion sensors may not be sufficient to monitor metropolitan areas for smart city applications.

New methodologies for ground-motion sensing using infrastructure that is already in place offer opportunities to lower costs and expand coverage in smart cities. One type of ground-motion monitor that has been proposed includes the use of accelerometers on mobile phones reported by Reilly *et al.* (2013). Although this approach is technically feasible, it requires users to install an app on their phone, and raises pri-
3 vacy concerns because an individual's location and activities would be monitored. Another approach is based on deployment of fiber-optic cable. Multiple studies have demonstrated the feasibility of using fiber-optic cable to monitor activities and events such as passing traffic or earthquakes (Ajo-Franklin *et al.*, 2019; Lindsey *et al.*, 2020; Shen and Zhu, 2021). Most of these studies use a technique called distributed acoustic sensing (DAS), which can be deployed on existing unused telecommunications fiber-optic infrastructure without interrupting the standard data transmissions (Martin *et al.*, 2017; Zhu *et al.*, 2021). A significant advantage of DAS versus traditional sensors is that it enables sensing along the entire length of a fiber with a spatial resolution of a few meters, thus dramatically increasing the sensor density and area that can be monitored. Although DAS has been shown to be a highly effective sensing technology and fiber-optic cables are already densely deployed in metropolitan areas (thus alleviating the need to install new infrastructure), the question remains of how to quantify the expansion of the monitored area by augmenting the existing ground-motion sensing arrays with fiber-optic cable-based sensor networks in smart cities. Our objective in this study is to address this question. We propose a methodology for assessing the expansion of monitored area by deploying ground-motion sensing capabilities along the fewest existing fiber-optic cables to augment sensing capabilities in smart cities. Identifying the fewest number of fiber segments that provide the largest new coverage area is critical to the economic success of large-scale deployments of ground-motion sensing on fiber-optic cables. Considerations for this sensing strategy include the cost of a DAS interrogator (which are currently about 10× the cost of a traditional point sensor, but it can sense more than 10^4 channels along over 10 km of the fiber) and the amount of data that must be processed. By identifying the fewest new fiber segments that require sensing capabilities, we minimize the cost to deploy this capability, as well as the amount of data that must be processed and stored.

Our methodology uses a geographic information system (GIS) to spatially analyze maps of metropolitan areas, locations of dedicated seismic sensors, and deployed fiber-optic cable. Specifically, we use GIS to spatially analyze these different information layers and quantify the spatial relationship of the sensor coverage area from existing seismic sensors augmented by data acquired by sensors deployed on the fiber-optic cable.

We first gathered the location information for metropolitan areas in the United States, existing networks of seismic sensors, as well as operational fiber-optic cable in the United States. We extended this information with noise levels observed at existing seismic sensors to calculate sensing coverage areas. We use the model by Wilson *et al.* (2021) to map the noise levels observed at each sensor to identify the detection threshold ranges, that is, the area around a sensor in which a ground-motion event could be detected above the background noise levels without human interpretation. In this research, we consider detection
areas for ground-motion events with magnitude M 0.5 (i.e., 4
very small events such as trains passing) and higher, (Earthquakes are measured by magnitude [M], which describes the size of the earthquake based on the physical characteristics of the emitted waveforms, U.S. Geological Survey [USGS] Earthquake Hazards Program, 2023.) We also applied this technique to the linearly distributed sensors, such as those that could be constructed by deploying DAS on existing fiber-optic infrastructure. Finally, we determined the optimal deployment of ground-motion sensors on existing fiber infrastructure to maximize the coverage area when using the fewest number of fiber-optic cable segments.

We utilize our technique to assess the combinations of existing dedicated seismic sensors and hypothetical arrays of sensors based on existing fiber-optic cable in the 100 most populous metropolitan statistical areas (MSAs) in the United States. Our analysis shows that there are an average of three seismic point sensors currently deployed in each MSA. On average, these seismic sensors can detect ground-motion events of magnitude M 0.5 in about 1% of an MSA's area. In contrast, we find that if all the fiber-optic cables in each MSA were used as sensors, on average, low-magnitude ground-motion events could be detected in 19% of the MSA's total area. We also find that if both the existing point sensors and sensors deployed on all the fiber-optic cables were utilized in an MSA, on average, low-magnitude events could be detected in 2200 km^2 (20%) of an MSA's total area. Finally, using an optimal selection technique to limit the number of fiber-optic cable segments required, on average we find that 1400 km^2

(12%) of each MSA could be covered by either a fiber-optic sensor or an existing seismic sensor.

We highlight the details revealed by our technique through specific examples of the spatial relationships for the Little Rock, Arkansas, and Seattle, Washington, MSAs. These examples allow us to visualize the sensor coverage areas when existing point sensors and sensors deployed on fiber-optic cables provide complementary coverage. We also use these MSAs to demonstrate the utility of the optimal deployment strategy by showing how many fiber-optic cable segments overlap and how we can still obtain significantly better coverage using a limited number of new sensors deployed on a fiber-optic cable.

Related Work

This research benefits from previous work in several different areas of study, including smart cities, ground-motion sensing, DAS, internet photonic sensing (IPS), and GIS-informed sensor placement.

Our study is inspired by the idea of the smart city. Smart cities are urban areas that use technology and data from multiple data streams to enable the effective city governance and improve the quality of life in diverse areas of public interest, for example, increase efficiency, improve sustainability, or
5 reduce costs. Technology use often includes using sensors and internet-connected devices to monitor and manage vehicular traffic from Rizwan *et al.* (2016), energy use from Mahapatra *et al.* (2017), waste from Nirde *et al.* (2017), and Aazam *et al.* (2016), and infrastructure health from Adedeji *et al.* (2022), as well as using data analytics to improve decision-making and public services from D'Aniello *et al.* (2020). Related research explores using smartphones to detect seismic activity for early warning systems reported in Kong *et al.* (2016). Although previous studies have identified many different benefits from using internet-connected devices and sensors for a variety of use cases in cities, none have attempted to quantify the extent of which currently deployed internet infrastructure could be used to improve the ability to understand urban area activities.

Ground-motion sensing refers to the measurement of the time history of ground vibration. This type of measurement includes sensing of earthquakes, construction and mining activities, for example, Mendecki (1996), and subsidence or slope failure, for example, Liang *et al.* (2013). Measurements of these motions are taken by a variety of types of sensors. The U.S. Geological Survey (USGS) typically uses three types
6 of sensors as components of the Advanced National Seismic System: broadband, short-period, and strong-motion sensors, Working Group on Instrumentation, Siting, Installation, and Site Metadata (2008). Broadband sensors measure the seismic motions with wide frequency and amplitude limits. Short-period sensors have limited bandwidth and are typically limited to frequencies above ~1 Hz. Strong-motion sensors measure large-amplitude motions. In addition to sensors used as a part of the national and regional networks, the studies have shown that microelectromechanical system accelerometers 7
may be used as lower-cost seismic sensors reported in Fu *et al.* (2019) and Cascone *et al.* (2021). The point sensors typically used in seismic monitoring networks are widely deployed, and our study seeks to understand how their monitoring capacity could be augmented to detect low-magnitude events in smart cities using linear sensors based on deployed internet fiber-optic cable.

In addition to using dedicated seismic sensors, many researchers have proposed using fiber-optic cable to detect ground-motion events. This is argued to be especially useful in areas where traditional seismic sensor deployment may prove difficult, such as metropolitan areas. One such technique is DAS reported from Parker *et al.* (2014) and Lindsey *et al.* (2017). DAS uses fiber-optic cables as sensors to detect, locate, and measure acoustic waves along the length of a cable. The technology works by sending rapid pulses of the laser light at regular intervals and then measuring the Rayleigh backscattered light using a photodiode that is collocated with the laser. Disturbances in the fiber such as acoustic waves, temperature changes, and mechanical vibrations create small changes in the position of scatterers in the fiber leading to a change in the backscattered wavefield that can be detected and converted into the measurements of strain along a cable (This is similar to optical time-domain reflectometry [OTDR], which is commonly used to detect and locate faults in optical fiber, but does not detect strain.). In addition to DAS, which commonly uses dedicated fiber-optic cable, IPS has been proposed to use existing fiber-optic cable from internet service provider (ISP) networks reported in Patnaik *et al.* (2021). Whereas DAS requires a dedicated interrogator unit to be deployed, IPS proposes utilizing existing internet optical transport hardware to detect strain on fiber. Initial results of IPS efficacy have been reported in Catudal *et al.* (2023). Both DAS and IPS demonstrate that it is possible to use a fiber-optic cable as a ground-motion sensor. Additional research showed the possibility of using existing fiber-optic cable in urban areas as a component of the smart city reported in Zhu *et al.* (2021). Our research provides a quantitative analysis of how far sensor networks' range could be extended when complemented by ground-motion sensors deployed on existing ISP networks.

Finally, our work is informed by prior studies that have utilized GIS to consider how to distribute sensors for monitoring the applications. The problem of geosensor deployment for environmental monitoring has been addressed in a number of prior studies. Argany *et al.* (2011) present a survey of techniques for optimized geosensor network deployment that are 8
based on utilizing Voronoi diagrams and Delaunay triangulation. More recently, a smart city-related study considered how to utilize GIS in conjunction with data from structural sensors to assess the integrity of bridges in areas of seismic activity reported by Malekloo *et al.* (2020). Although these studies

provide useful perspectives, we are not aware of any prior work that considers how GIS can be used to assess the expansion of ground-motion monitoring via internet fiber infrastructure.

Data sets

To conduct our study, we utilized multiple data sources on the spatial extent of metropolitan areas, internet fiber-optic cable, and existing ground-motion sensors. We analyzed these data sets as spatial layers using GIS to assess the extent to which ground-motion sensing capability can be expanded via existing fiber infrastructure.

To capture the spatial extent of metropolitan areas, we used the U.S. Census Bureau Cartographic Boundary Files reported
9 by U.S. Census Bureau (2023). These digital boundary files provide spatial limits for various geographic areas, including states, counties, census tracts, and block groups for the United States. These files are designed to be used with GIS software and other mapping programs for spatial analysis. Because of our interest in smart cities, we used the MSA shapefiles, which encompass city administrative boundaries as well as the surrounding area that is economically and culturally similar to the central metropolitan area. Note that this design choice leads to conservative results on expanded coverage for smart cities because in most cases, MSA boundaries extend beyond the city limits.

For a spatial understanding of in-use ISP fiber-optic cable infrastructure, we used the Internet Atlas metropolitan fiber-optic cable shapefiles reported by Durairajan *et al.* (2013). Internet Atlas was a research project that aimed to map the
10 physical infrastructure of the internet, including points of presence, fiber-optic cable, and other key components of internet physical infrastructure. This information improves the understanding of the internet's topology and to identify potential bottlenecks and vulnerabilities. Internet Atlas includes metro fiber maps for the 100 most populous MSAs considered in our study (except Honolulu, Hawaii). Although these maps cannot be guaranteed to be complete, they are the most accurate source of shapefiles of metro fiber infrastructure deployment that is openly available for research.

Finally, we obtained information on ground-motion sensors from the Incorporated Research Institutions for Seismology (IRIS) database, which includes data from seismographic stations around the world reported by Incorporated Research Institutions for Seismology [IRIS] Consortium (2023), including those that are part of the IRIS Global Seismographic
11 Network. This database includes fields on sensor network, location, instrument type(s), site name, time period a sensor was active, as well as information about the sensor measurements including noise. The Data collection section describes how we accessed, filtered, and processed the available data.

Methodology

To assess how seismic sensing coverage can be extended by deploying sensors on internet optical fiber in smart cities, our methodology uses ArcGIS and GeoPandas to process multiple layers of geospatial data reported by ESRI (2020) and GeoPandas (2023). In the following sections, we describe our methodology in detail.

Data collection

As described in the Data sets section, we directly accessed MSA boundaries and fiber-optic cable shapefiles. MSA boundaries are stored as multipolygon shapes in the shapefile, which also includes administrative information such as MSA name and population. The fiber-optic cable shapefile included all known fiber-optic cable in the United States from Internet Atlas, stored as line shapes. Although the fiber-optic cable shapefiles accurately describe the spatial layout of fiber-optic cables, they do not necessarily reflect which cable segments were physically connected. The fiber-optic shapefiles also do not include administrative information such as the ISP name. For our research, a cable segment is a single spatial linestring from the transcribed map. Each cable segment represents the physical pathway that the ISP fiber-optic cable followed, but, without access to additional proprietary ISP infrastructure maps, we cannot confirm that each linestring represents a single fiber-optic cable or that each fiber-optic cable is represented by a single linestring. Finally, at the metropolitan level, these linestrings show the path that the fiber-optic cable followed, but do not necessarily represent the logical connection of nodes and end points in the metropolitan area. Although the Internet Atlas study originated to elucidate the physical connectivity in the internet, new, focused studies on using fiber-optic cable for ground-motion sensing could show deployment characteristics relevant to using fiber as a sensor, such as (1) how actual fiber routes diverge from cable maps; (2) locations of fiber slack loops and transceivers; and (3) observed noise on each segment reported from Cunningham *et al.* (2022).

In contrast, we had to process information about sensor locations and noise to make it spatially relevant to the MSA and fiber location information. We first downloaded seismic sensor names, networks, and locations (latitude/longitude coordinates) for sensors in the United States from the IRIS Gmap reported by IRIS Consortium (2023). This information included sensors that were no longer active as well as sensors that were planned for future deployment. We processed these data to limit our results to active sensors then used GeoPandas to process the flat latitude/longitude coordinates into geospatial point shapes. In addition, for each seismic sensor, we required seismic noise data. Because we considered hundreds of seismic sensors across the entire United States, we collected noise information for each sensor of interest for a 24-hr period, 14 June 2022, a typical Tuesday without global large-magnitude earthquakes. Noise information is provided for the three spatial components: north–south, east–west, and vertical for discrete frequencies in the range of 0.005–50 Hz. Specifically, we collected noise measurements from broadband and

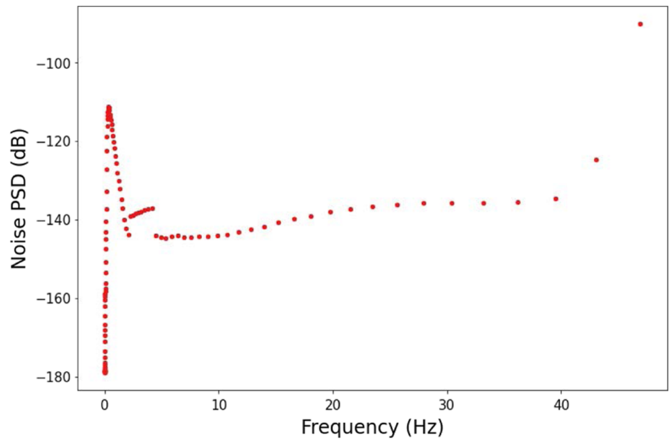

30 **Figure 1.** Observed noise on 14 June 2022 across frequencies at the Baber Butte, Oregon, seismic sensing station (BABR). The color version of this figure is available only in the electronic edition.

high-broadband, high-gain seismometers in the vertical orientation. Because different types of sensors are sensitive to different frequency ranges, we therefore limited our analysis to a narrowband around 10 Hz, a common frequency across sensor types and low enough to be emitted by low-magnitude seismic events.

Events of interest for smart city detection produce ground vibrations with dominant energy sources across multiple frequency ranges: vehicle transportation and cultural noise (surface waves 1–500 Hz), industrial and mining activity (5–1000 Hz), blasting (1–100 Hz), local (5–60 Hz), and regional (0.1–20 Hz) earthquakes reported in Schwardt *et al.* (2022). The average normalized spectra for blasts and earthquakes is between 10 and 20 Hz (e.g., Kim *et al.*, 1994) and for vehicles at distances 10–100 m away from the sensor is between 10 and 15 Hz (e.g., Long, 1993). The energy in the average spectra for sources such as blasts and vehicles decrease with distance for higher frequencies due to attenuation (e.g., Kenney, 1977; Meng *et al.*, 2021; Zhao *et al.*, 2023), and we expect persistent ambient noise at lower frequencies, as seen at <1 Hz in Figure 1. With that background on frequency ranges for events of interest in mind, the IRIS data set includes noise PSD for each channel at discreet frequency intervals, for example, 1.03747, 5.38174, 10.7635, 23.4753 Hz, and so forth, as seen by each point in the plot in Figure 1. Taking into account the sensors and events of interest, we chose to evaluate the noise at a frequency of 10.7635 Hz, a frequency common to all sensors of interest. Given a more specific target event, the center frequency could be modified.

Calculating detection threshold

With the noise data collected for each point sensor, we calculate the automatic detection threshold using the technique from Wilson *et al.* (2021), which we describe briefly here. Wilson *et al.* (2021) noted that the automatic detection threshold for seismic sensors varies based on the observed noise levels (which can vary greatly among different sensors) as well as temporally at the same sensor. The automatic detection threshold refers to the lowest-magnitude seismic event that is sufficiently above the noise floor for algorithmic identification.

From their empirical study of historical events and background noise levels, Wilson *et al.* (2021) developed a model that took as an input the background noise at a sensor as well as a user-provided distance from the sensor to predict the lowest-magnitude event that could be detected at that distance. We reproduced these in equations (1), (2), and (3), in which R is the distance from sensor (in kilometers), M is the detectable magnitude, and N is the sensor noise level (in decibels):

$$\text{if } R < r_1 : M = a_1 \log_{10}(R) + b_1 R + dN + c, \tag{1}$$

$$\begin{aligned}\text{if } r_1 < R < r_2 : M = {} & a_2 \log_{10}(R/R_1) + a_1 \log_{10}(r_1) \\ & + b_2(R - r_1) + b_1 r_1 + dN + c,\end{aligned} \tag{2}$$

$$\begin{aligned}\text{if } R > r_2 : M = {} & a_3 \log_{10}(R/r_2) + a_2 \log_{10}(r_2/r_1) + a_1 \log_{10}(r_1) \\ & + b_2(r_2 - r_1) + b_1 r_1 + dN + c.\end{aligned} \tag{3}$$

We used the coefficients for P waves calculated by Wilson *et al.* (2021) and reproduced in Table A1. One limitation of our 12 technique is that these coefficients were calculated for the central United States, but we use them uniformly throughout metropolitan areas in the United States. Although this is appropriate to show the feasibility of using a technique like DAS deployed on optical fiber, more regionally aligned coefficients should be calculated and used to determine more exact detection threshold areas. In our study, we adapted these equations to determine the farthest distance that a ground-motion event at a given magnitude could be detected from a given sensor.

Each sensor has distinct noise threshold characteristics in both frequency and time. Figure 1 shows an example of how noise levels vary across frequencies for a sensor at the Baber Butte, Oregon, seismic sensing station (BABR), and Figure 2 shows how noise varies across a 24-hr period. Note that these two patterns are not necessarily representative for all sensors. Similar to Figure 1, many sensors have a frequency for which the noise is lowest. However, in contrast to Figure 2, the lowest recorded noise levels for some sensors occur during periods of minimal anthropogenic activity, that is, at night. Because the noise levels vary, we calculated the average noise level over a 24-hr period for each sensor. However, other aggregations of observed noise at a sensor (e.g., min or max) could be used for other use cases.

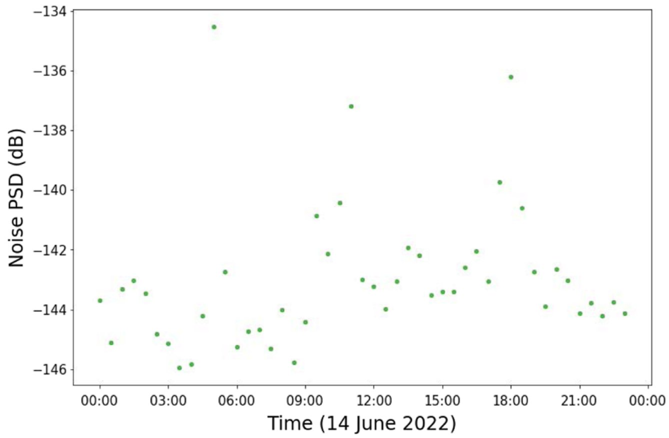

Figure 2. Observed noise on 14 June 2022 for frequency 10 Hz at the Baber Butte, Oregon, seismic sensing station (BABR). The color version of this figure is available only in the electronic edition.

Ground-motion events produce seismic waves in all three spatial directions (north–south, east–west, and vertical). Our methodology could be used for analysis of different types of seismic waves (i.e., surface waves, *P* waves, or *S* waves) and may incorporate noise measurements from any spatial direction. For this study, we use noise measurements along the vertical direction because teleseismic *P* waves have a strong vertical component. Because *P* waves travel faster than *S* waves, they are important for seismic activity detection and early warning systems reported in Allen *et al.* (2009). Using the appropriate equations to calculate detection thresholds from noise measurements, our methodology could also be applied to surface waves from shallow sources, which have greater amplitudes and longer periods than *P* waves, which is useful for monitoring near-surface events.

We use the average noise and desired seismic event magnitude to calculate the radius around each sensor within which any seismic event of that magnitude or greater could be automatically detected. We use this radius to spatially generate a buffer around the sensor in a GIS. For point sensors, such as traditional seismic sensors, this buffer corresponds to a circle around the sensor. For ground-motion events with magnitude greater than M 2.0, the events could be detected hundreds of kilometers from a sensor. This leads to complete and overlapping coverage for most MSAs. However, lower-magnitude events may be detected only when they occur much closer to a sensor. For example, the seismic sensor with the lowest average noise power spectral density (PSD) (−150 dB) could detect M 0.5 seismic events within 30 km and M 1.5 events within 200 km. The average noise PSD at 10.7635 Hz was −121.5 dB. On an average, a sensor could detect M 0.5 events out to 2.3 km and M 1.5 events within 65 km of the sensor. We assume that detection thresholds around a sensor are uniform, that is, they form a circle around the sensor within which all the seismic events of that magnitude or greater could be detected.

To compare the detection coverage of dedicated seismic sensors to sensors using fiber-optic cable, we must develop a convention for the detection threshold of fiber-optic cable. One consideration for the detection threshold is the directional sensitivity of DAS. In particular, DAS is sensitive to axial strain on a fiber, so deliberately placed DAS arrays often use specific geometric arrangements of the fiber-optic cable (Wang *et al.*, 2018; Wuestefeld and Wilks, 2019). Although existing fiber-optic cable does not necessarily follow the same geometric patterns as a deliberately-placed DAS array, it is often run in a multidirectional pattern, which would provide complete coverage around the fiber segments.

Many studies have been conducted that document the detection thresholds of DAS arrays on both dedicated fiber-optic cable deployments and over existing fiber-optic networks to detect seismic and anthropogenic events. For example, deliberately-placed fiber-optic networks have been used as DAS arrays to detect an M 3.8 seismic event 150 km away and an M 5.8 event over 2000 km away in Lindsey *et al.* (2017), an M 4.3 earthquake with epicenter about 150 km away in Wang *et al.* (2018), as well as an M 2.0 earthquake detected 5.2 km away and an M 5.8 earthquake 182.6 km away in Yin *et al.* (2023). In addition, Wang *et al.* (2020) demonstrated the ability to detect parade foot and vehicle traffic within 2.5 km of a DAS array deployed on existing telecommunications fiber-optic cable. Finally, Li *et al.* (2021) used DAS on existing telecommunications fiber-optic cable to detect M 2–3.5 aftershocks within 20 km of the array. In addition to these focused studies, efforts are underway to make DAS data more widely available, for example, through PubDAS in Spica *et al.* (2023). Despite these efforts, there is no comprehensive set of detection thresholds or noise measurements for all the telecommunications fiber-optic cables considered in this study. Therefore, we adopt a uniform, conservative estimate for the detection threshold of sensors in fiber-optic cables.

We use 1.5 km as the detection threshold of sensors in fiber-optic cable for events of M 0.5 or greater, which is well below the average detection threshold for dedicated seismic sensors and in agreement with the studies listed in the previous paragraph. We anticipate refining this estimate with future sensor deployments using fiber-optic cables, including the ability to measure individual noise levels for different fiber-optic cable segments.

We concentrate on M 0.5 events for our analysis because seismic sensors are geographically widespread enough to detect events of larger magnitude, and the anthropogenic events we focus on in smart cities will only produce very low-magnitude ground motion. However, our methodology is robust enough to be applied for smaller- or larger-magnitude events as desired.

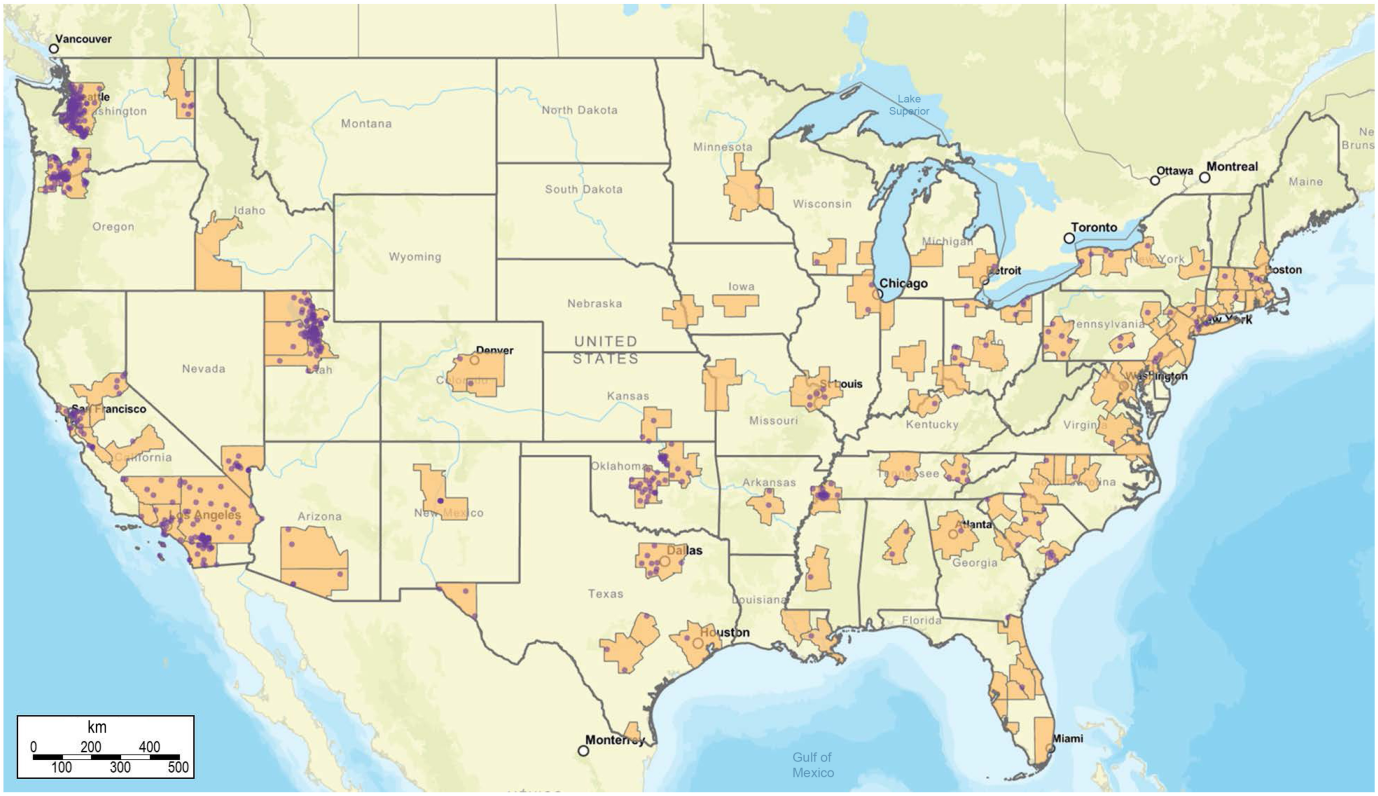

Figure 3. Geographic distribution of the 100 most populous metropolitan statistical areas (MSAs) in the United States (orange polygons) along with the active dedicated seismic sensors in each MSA (purple points). The color version of this figure is available only in the electronic edition.

Detection threshold buffers around point sensors are uniform circles of radius detection threshold distance with the sensor as the center of the circle. In contrast, for linearly distributed sensors based on fiber-optic cables, the detection threshold buffer is an irregular polygon enclosing the linear sensor in which the polygon edge is detection threshold distance from the linear sensor.

Conducting spatial analysis

Our methodology uses average noise measurements to calculate the radius of the detection threshold for a single point or linearly distributed sensor, and then determine a buffer area around the sensor. Calculating the coverage of a set of sensors within an MSA requires a spatial analysis that accounts for the geographic location of sensors, the irregular perimeters of MSAs, as well as the extent of the sensor coverage area. For this, we considered multiple layers of data to spatially understand the relationships using a GIS. Specifically, we considered the following layers of data: fiber-optic cable from Internet Atlas (linestring data), MSA perimeters from the U.S. Census Bureau (multipolygons), location of ground-motion sensors from IRIS (point data), and perimeters of detection areas—calculated using the methodology outlined above—for dedicated seismic sensors and fiber-optic cable (multipolygons).

We identified the largest MSAs by population by joining two data sources from the U.S. Census Bureau: the MSA geographic shapefile and a table of MSA populations reported in U.S. Census (2023). For each MSA, we then conducted spatial joins with the fiber-optic cable and seismic sensor location shapefiles to identify the fiber and sensors within each MSA. The MSA extent and sensors within the 100 most populous MSAs are shown in Figure 3.

For the fiber and sensors within an MSA, we used the detection threshold radius for M 0.5 ground-motion events to create layers with spatial buffers around each fiber segment and each sensor. The equations assume that the sensors have circular buffers created from variable-length detection threshold radii, whereas the fiber had irregular polygon buffers that followed the fiber route. Where detection threshold buffers exceeded the MSA perimeters, we spatially truncated the buffers to limit them to the spatial extent of the MSA polygon.

With the detection threshold buffers for dedicated seismic sensors as well as for fiber-optic cable, we next determined the total coverage area within each MSA. We accounted for overlapping coverage areas in the following manner: we first spatially dissolved the sensor buffers to remove overlap in coverage, then we spatially dissolved the fiber-optic cable buffers. Finally, we gave precedence to existing seismic sensor coverage area and we remove any overlapping coverage area from the fiber buffers. With the buffers thus prepared, we used the GIS to calculate the areas of the MSA, fiber buffer coverage, and point sensor buffer coverage.

One consideration with the total coverage area calculations described earlier is that they permit overlapping detection coverage without penalizing for sensors with overlapping coverage that does not improve the overall spatial coverage in the MSA. Deploying new sensing capabilities in fiber-optic cables could be costly in terms of equipment required, labor costs to install, as well as in operating costs. Therefore, we needed a method to determine the largest coverage area while reducing the number of fiber-optic cable segments that require installation of new sensing capabilities, a standard minimax problem. For this, we first spatially created the detection threshold buffers around each fiber-optic cable segment and seismic sensor for an MSA, as described earlier. However, we maintained each detection threshold buffer around the fiber-optic cable segments as a separate polygon shape and did not dissolve the polygons around each fiber segment into a single shape. In this manner, we determined the detection area around each fiber segment if we installed a sensing capability in that fiber-optic cable segment.

Next, we spatially identified and removed any fiber detection buffer from consideration that overlapped with any point sensor buffer. Because dedicated seismic sensors are already in place and have been deliberately deployed, there is no increase of the spatial coverage area if additional sensing capability was deployed in a fiber-optic cable in that area (although some point sensors could potentially be decommissioned for a minimal reduction in operating costs). After removing these fiber detection buffers from consideration, we next took a greedy approach to identify the largest coverage area possible using the fewest number of new sensors in fiber-optic cable. We sorted all fiber detection buffers that did not overlap with the dedicated sensor buffers from the largest area to smallest and then iterated through each fiber buffer. We started with an empty set of optimal fiber detection coverage. At each step, if the fiber buffer under consideration did not overlap with any buffer in the optimal fiber detection coverage set, we added that buffer to the optimal fiber detection coverage set. In this manner, we significantly reduced the number of new sensors required for deployment on deployed fiber, while maintaining robust ground-motion detection coverage throughout most MSAs. We demonstrate the effectiveness of this strategy in the Results section.

Results

Spatial analysis of largest MSAs in the United States

Of the 100 most populous MSAs considered in our analysis, the largest (New York–Newark–Jersey City) has a population of over 20 million people, whereas the smallest (Scranton–Wilkes-Barre, Pennsylvania) has a population of just over 565,000. The average population of the 100 most populous MSAs is 2,200,000. Table A2 shows the ten largest MSAs by population. By area, MSAs range in size from 71,000 km^2 (Riverside–San Bernardino–Ontario, California) down to 1,600 km^2 (New Haven–Milford, Connecticut), with an average area of 12,000 km^2.

Figure 3 shows the 100 most populous MSAs along with the active dedicated seismic sensors within MSA boundaries. When considering currently deployed dedicated seismic sensors in the 100 most populous MSAs, on an average there are three sensors per MSA. There are 30 MSAs with no active dedicated seismic sensors. There are seven MSAs with ten or more active dedicated seismic sensors, enumerated in the Appendix. Across all the 100 most populous MSAs, our analysis shows that on an average, seismic sensors can detect low-magnitude ground-motion events in 1% of an MSA's area. Albuquerque, New Mexico, has the most area covered by seismic sensors, with 2800 km^2 (12%) of the land area covered by active dedicated sensors.

Recognizing that 30 of the 100 most populous MSAs do not have any active seismic sensors, and that the MSAs with dedicated sensors can detect low-magnitude ground-motion events in only about 1% of the total area, there is much opportunity to expand the sensor coverage area. If all the fiber-optic cables in each MSA were used as sensors, when considering low-magnitude (M 0.5) ground-motion events, our analysis shows that, on average, 19% of the MSA total area could be covered. New Haven–Milford, Connecticut, has the smallest area within which an event could be detected (54 km^2) by fiber-optic cable sensors. This is only 3% of the total MSA area of 1600 km^2. In contrast, by the percentage of MSA covered, Cleveland–Elyria, Ohio, has the largest area that could be covered by fiber-optic cable sensors (40%). Atlanta–Sandy Springs–Alpharetta, Georgia, has the next largest area that could be covered by fiber-optic cable sensors: 8,600 km^2, which is 38% of the total MSA area (23,000 km^2).

Next, we assess how ground-motion sensors deployed within existing fiber-optic cable could complement dedicated seismic sensors. On an average, a combination of dedicated seismic sensors and sensors using fiber-optic cable could detect low-magnitude events in 2200 km^2 (20%) of an MSA's total area. In the best case, Dallas–Fort Worth–Arlington, Texas, MSA has the largest area (11,300 km^2 or 49%) that could be covered by fiber-optic cable and seismic sensors.

Because of the abundance of fiber-optic cable in different MSAs that could be harnessed for seismic sensing, it is important to identify the fewest fiber-optic cable segments that provide the largest coverage area, without overlapping coverage areas. Using this technique, on an average 1400 km^2 (12%) of each county could be covered by either a fiber-optic sensor or a dedicated seismic sensor.

Our results across all the MSAs are summarized in Table 1. See Table A3 for a list of results for the 75 most populous MSAs.

Spatial analysis of Little Rock, Arkansas

Focusing attention on a specific MSA allows us to better understand the spatial relationships of an MSA in which

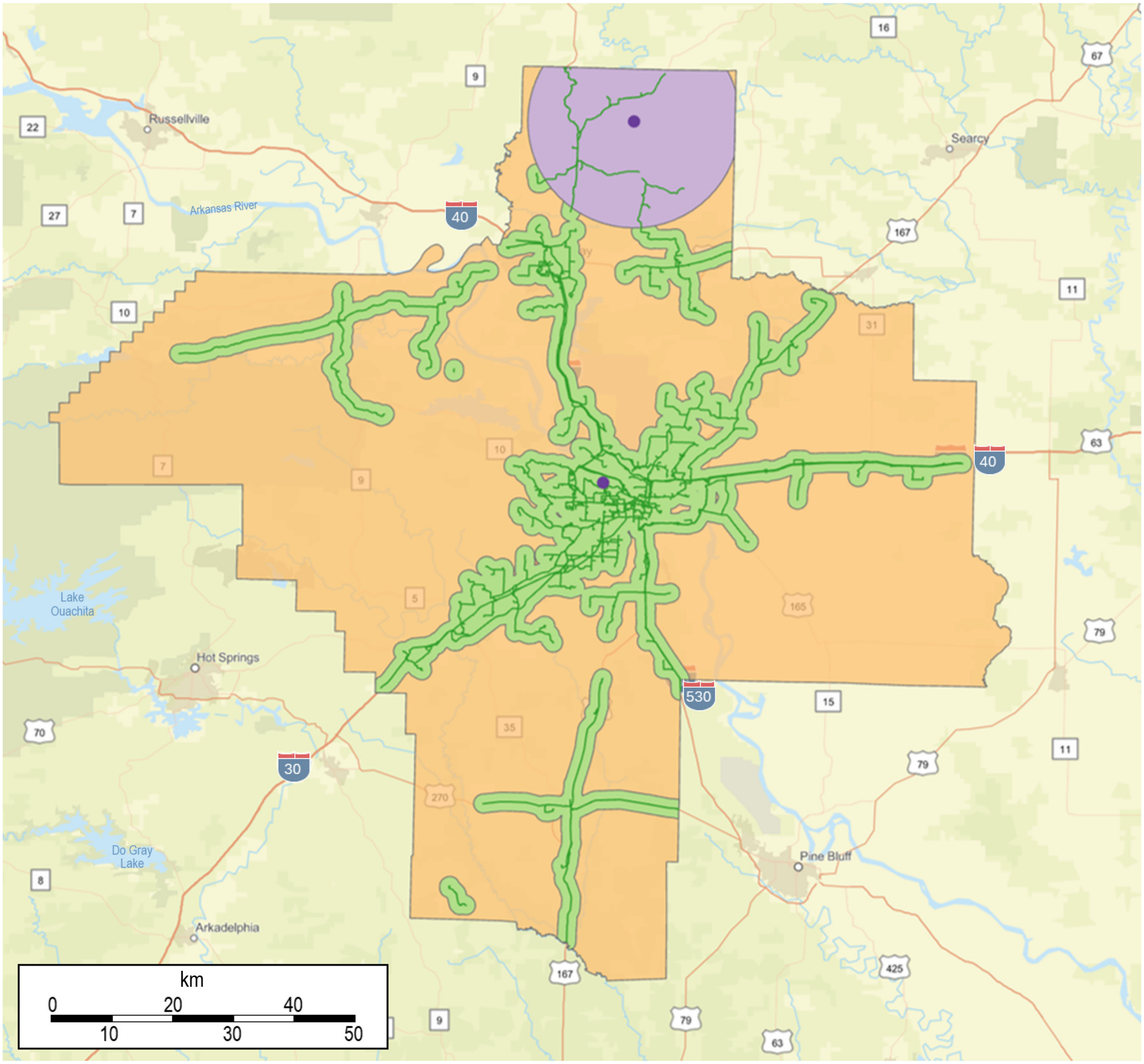

low-magnitude ground-motion events could be detected by dedicated seismic sensors, by sensors deployed on fiber-optic cable, and by sensors only placed in an optimal fashion within the fiber-optic cable. We chose Little Rock, Arkansas, for our first case study because of its proximity to the New Madrid Seismic Zone (NMSZ) reported by Missouri Department of Natural Resources (2023) and because of the illustrative characteristics of seismic sensors and fiber-optic cable in the MSA. The NMSZ is a region in the central United States, spanning parts of Missouri, Arkansas, Tennessee, Kentucky, and Illinois, where a high level of seismic activity has been recorded. Because the NMSZ is one of the most active seismic zones in the central and eastern United States with the potential to damage heavily-populated areas, it is closely monitored by the U.S. Geological Survey (USGS) (2023). Because large-magnitude earthquakes are infrequent, the structures are not always consistent with the latest seismic building codes. Therefore, damage from a large-magnitude event could be extremely costly. Ambient noise tomography, using improved sensing coverage and traffic as a noise source, can be used to obtain near-surface shear-velocity profiles and to compute engineering parameters such as V_{S30}, the average S-wave

Figure 4. Geographic extent of the Little Rock, Arkansas, MSA (orange polygon) with existing dedicated seismic sensor coverage for low-magnitude events (purple buffer), existing internet service provider (ISP) fiber-optic cables (green lines), and potential detection area for low-magnitude ground-motion events using fiber-optic cable as sensors (light green buffer). The color version of this figure is available only in the electronic edition.

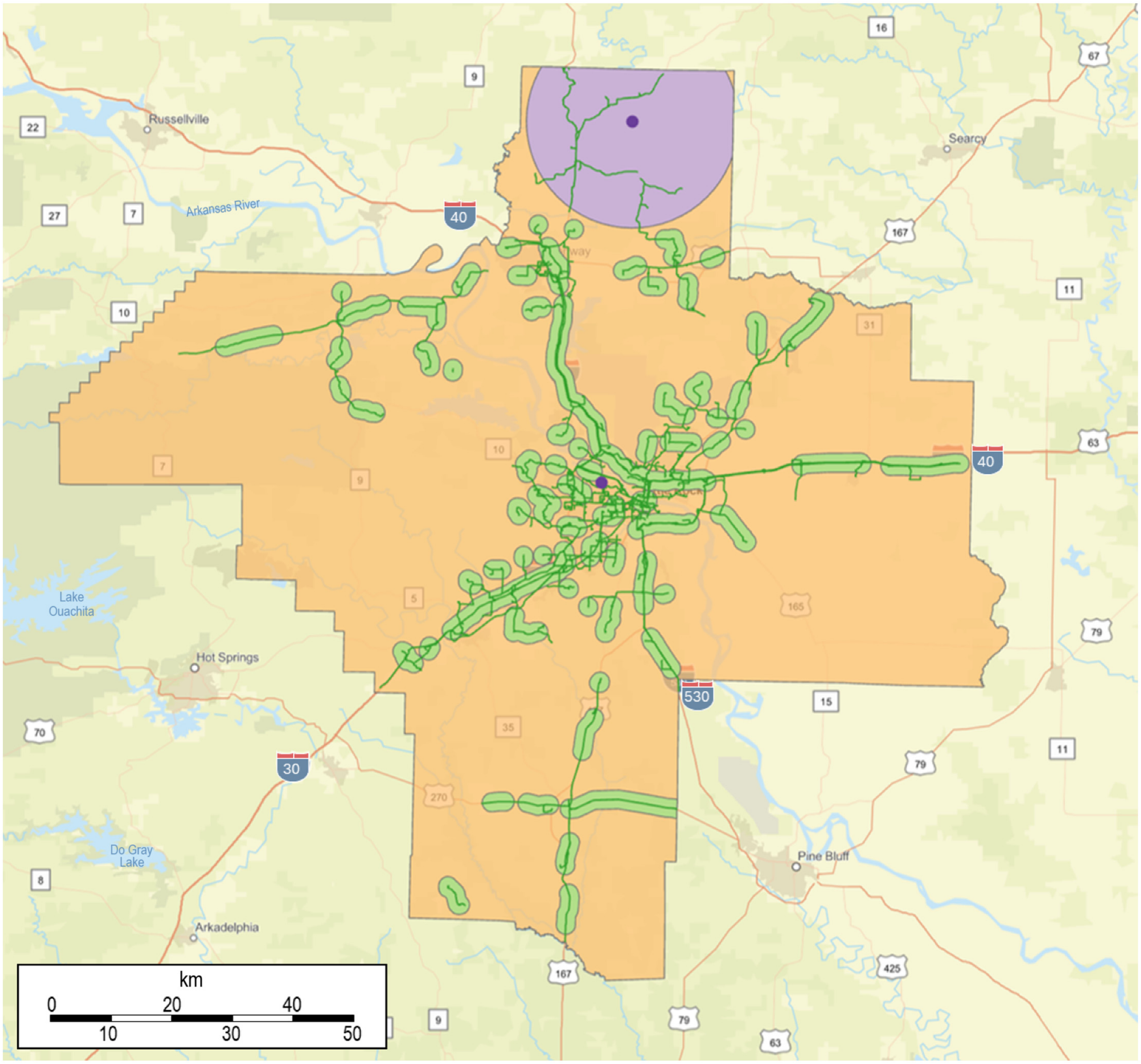

velocity in the top 30 m. This can help define which areas are the most vulnerable.

The Little Rock, Arkansas, MSA includes the city of Little Rock and the surrounding area, including Pulaski County, covering 10,933 km^2. There are two active dedicated seismic sensors in the MSA, shown as purple dots in Figure 4. The Woolly Hollow State Park, Arkansas, sensor (WHAR) from the Arkansas seismic sensor network is located in the northern part of the MSA, and the University of Arkansas, Little Rock, sensor (UALR) from the New Madrid (NM) seismic sensor network is located near the center of the MSA in the city of Little Rock.

Using the noise measurements described in the Data sets section, we calculated the maximum distance from each sensor in which a low-magnitude ground-motion event could be detected. Because of high noise around the UALR sensor (−127 dB), the detection radius was less than 0.5 km. However, the WHAR sensor had much lower noise at the sensor site (−143 dB) and, therefore, could detect low-magnitude seismic events in the 704 km^2 surrounding the sensor, as

Figure 5. Geographic extent of the Little Rock, Arkansas, MSA (orange polygon) with existing dedicated seismic sensor coverage for low-magnitude events (purple buffer), existing ISP fiber-optic cables (green lines), and optimal detection area for low-magnitude ground-motion events using fiber-optic cable as sensors (light green buffer). The color version of this figure is available only in the electronic edition.

TABLE 1

31 **Summary of Area in the 100 Largest Metropolitan Statistical Areas (MSAs) Within Which Low-Magnitude Seismic Events (M 0.5) Could be Detected Using Different Combinations of Ground-Motion Sensors**

Sensor Types	Average Area (km^2)	Percent of MSA Area
Existing seismic sensors	218	1.1
Fiber-optic cable	1975	18.7
Fiber and seismic sensors	2194	19.8
Optimal fiber and seismic sensors	1383	12.2

TABLE 2

Area of Little Rock Metropolitan Statistical Areas (MSA) Within Which Low-Magnitude Seismic Events (M 0.5) Could be Detected Using Different Combinations of Ground-Motion Sensors

Sensor Types	MSA Area (km^2)	Percent of MSA area
Existing seismic sensors	704	6.5
Fiber-optic cable	2565	23.5
Fiber and seismic sensors	3259	30
Optimal fiber and seismic sensors	2107	19.4

represented by the purple circle in Figure 4. This results in 6.5% of the Little Rock MSA having coverage from dedicated seismic sensors for low-magnitude events.

The fiber network in the Little Rock MSA, depicted by the green lines in Figure 4, is quite extensive. The center of the MSA is the city of Little Rock, with metropolitan fiber throughout the city. Long-haul fiber then runs from Little Rock to the north, east, and south along Interstate highways I40, I30, and I530 to smaller cities and towns, including Conway, Bryant, and Pine Bluff. We assume a high noise level around the fiber-optic cable, so the cable can be used to uniformly detect ground-motion events of M 0.5 within 1.5 km of the cable. Of note is that some of the possible coverage from using sensors on the fiber-optic cable in the northern part of the MSA would overlap with seismic sensor coverage already in place. We explicitly removed all fiber-optic coverage buffers that overlapped with existing seismic sensor coverage from consideration, with the expectation that any deliberately placed seismic sensor would provide more robust ground-motion detection than that placed using ISP fiber-optic cable. Our results show that 2565 km^2 (23.5%) of the MSA is within the low-magnitude ground-motion event detection threshold if all the fiber-optic cables were used for event detection. If both the deployed point sensors and fiber-based sensors were used, the coverage would expand to 3259 km^2 (30%) of the MSA.

However, this is an optimistic scenario that would require extensive resources to be deployed along many different fiber-optic segments and would result in a great deal of overlapping coverage without added spatial coverage. We therefore used the optimal analysis algorithm described in the Methodology section to determine that using only 72 of the 2452 fiber-optic cable segments in the MSA could provide detection coverage of 1407 km^2 (12.9% of the MSA). As shown in Figure 5, using this optimal number of fiber-optic cables provides 55% coverage of the total possible area using fewer than 2.9% of fiber segments. We summarized these results in Table 2.

Spatial analysis of Seattle, Washington

In contrast to the Little Rock MSA, the Seattle MSA is an area in which point sensors are much more widely deployed so selection to extend the coverage area would have to be considered more carefully. The Seattle, Washington, MSA covers 15,535 km^2 and encompasses the cities of Seattle, Tacoma, and Bellevue, as well as the surrounding commercial and industrial areas, and smaller communities.

There are 27 seismic sensing stations in the MSA, with most of the sensors outside of the major urban areas in the southeast area of the MSA. These sensors can be used to detect low-magnitude ground-motion events over 1005 km^2, which amounts to 6.5% of the MSA. As seen by the purple circles in Figure 6, many of the sensors are placed in close proximity, providing overlapping coverage areas. Because a demonstration of these sensors' ability to detect anthropogenic ground-motion events, one of these sensors, which is deployed in a large stadium (Kingdome, Seattle, Washington—KDK), detected crowd noise 13
during a sporting event in 2011 reported in Vidale (2011).

Similar to the dedicated sensors, much of the fiber-optic cable is located along the western part of the Seattle MSA. This reinforces our premise that because fiber is deployed in areas where people live, it offers a compelling opportunity for use in ground-motion sensing in a smart city. For low-magnitude ground-motion events, if sensors were deployed over the entire fiber network, the total area in which ground-motion events could be detected is 3046 km^2, which is 19.61% of the Seattle MSA.

It is important to note that much of this MSA is, in fact, rural, and the coverage in populated areas is much higher. Furthermore, because almost all the current seismic sensor coverage area is outside of the area that could be covered by sensors using fiber-optic cable, those sensors would significantly extend the coverage area throughout the MSA—especially in densely-populated urban areas. All dedicated seismic sensors and possible sensors in fiber-optic cable would cover 4052 km^2 (26.1%) of the entire MSA for low-magnitude events.

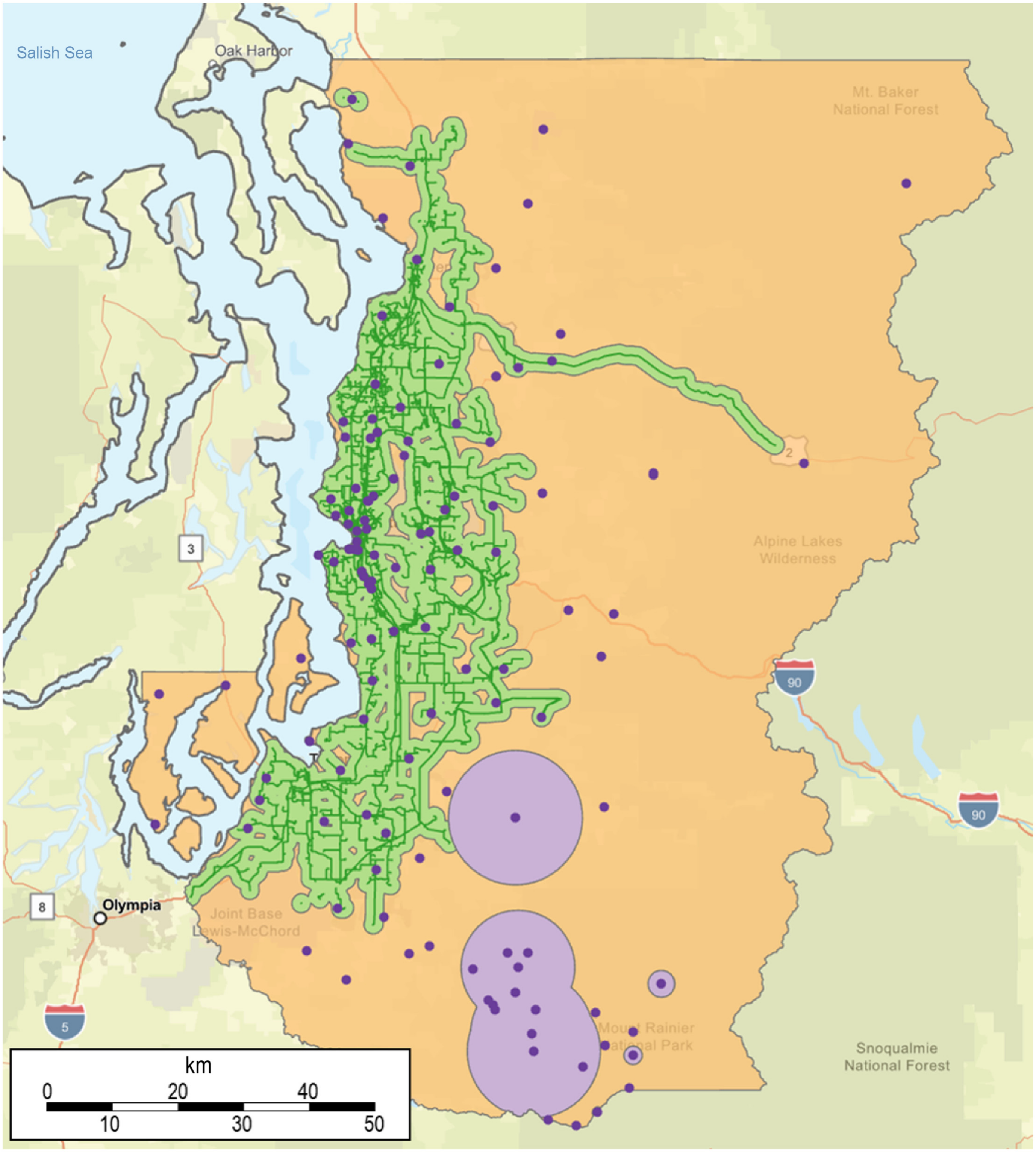

Figure 6. Geographic extent of the Seattle, Washington, MSA (orange polygon) with existing dedicated seismic sensor coverage for low-magnitude events (purple buffers), existing ISP fiber-optic cables (green lines), and potential detection area for low-magnitude ground-motion events using fiber-optic cable as sensors (light green buffer). The color version of this figure is available only in the electronic edition.

More conservatively, if we consider the scenario in which we only deploy new sensors on the fiber-optic cable in a manner in which the coverage area does not overlap, we still find significant gain as compared to only using currently deployed dedicated seismic sensors. As depicted in Figure 7, optimal placement of sensors using fiber-optic cable would provide nonoverlapping coverage of 1862 km^2 (12%) of the MSA. In this case, optimal

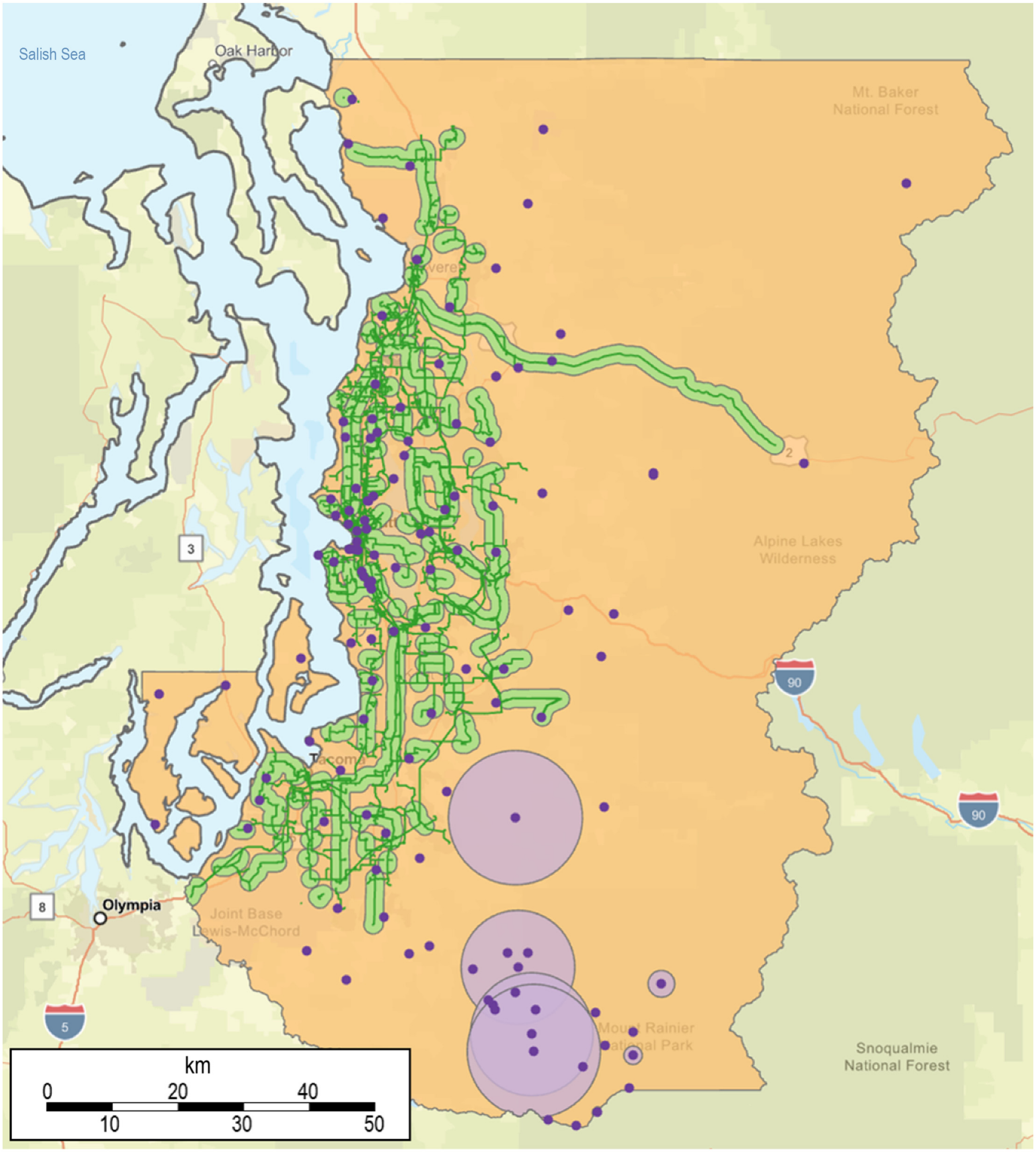

placement means using our greedy approach to install sensing capability on only 74 of the 16,052 total fiber segments (0.5%) in the MSA. Considering the total coverage area of optimal sensors using fiber-optic cable in addition to the existing sensor coverage area, we see 2868 km^2 (18%) of the MSA covered for low-magnitude ground-motion events. These results are summarized in Table 3.

Figure 7. Geographic extent of the Seattle, Washington, MSA (orange polygon) with existing dedicated seismic sensor coverage for low-magnitude events (purple buffers showing overlapping coverage area), existing fiber-optic cables (green lines), and optimal detection area for low-magnitude ground-motion events using fiber-optic cable as sensors (light green buffer). The color version of this figure is available only in the electronic edition.

TABLE 3

Area of Seattle–Tacoma–Bellevue Metropolitan Statistical Areas (MSA) Within Which Low-Magnitude Seismic Events (M 0.5) Could be Detected Using Different Combinations of Ground-Motion Sensors

Sensor Types	MSA Area (km^2)	Percent of MSA area
Existing seismic sensors	1005	6.5
Fiber-optic cable	3046	19.6
Fiber and seismic sensors	4052	26.1
Optimal fiber and seismic sensors	2868	18

Discussion

Our results highlight the compelling opportunities for smart cities and for equipment manufacturers to more widely use ISP fiber-optic cable as ground-motion sensors. In particular, our methodology enables city planners to assess and manage ground-motion sensing coverage while minimize deployment costs. Similarly, there has been a surge of companies developing DAS devices (e.g., Optasense, 2023; Silixa, 2023) over the past several years. Although there are compelling applications in commercial areas, our methodology and results can be used to motivate configurations for deployment for urban ground-motion monitoring.

Our calculations for the ground-motion detection coverage area for each fiber segment is a conservative estimate because, as far as we know, there have been no comprehensive studies of ambient noise for DAS deployed on ISP fiber-optic cables. More accurate noise measurements on fiber-optic cable segments would improve the accuracy of detection thresholds. With the noise measurements that we consider for point sensors, we average across a 24-hr period. Although we believe this is reasonable for our study, noise estimation could be more broadly considered using historical measurements from deployed sensors.

We used fiber-optic cable maps from Internet Atlas by Durairajan *et al.* (2013), which are the most accurate maps available for research and include data for over 200 MSAs in the United States. However, these maps may not represent all the fiber segments for all ISPs that operate in the 100 most populous MSAs. ISPs consistently deploy new optical fiber to improve the speed and reliability of their services. Although ISPs are typically reticent to share details of their infrastructures for competitive reasons, coverage analysis would be improved with the most comprehensive and up-to-date maps of fiber infrastructure deployments. In addition, these fiber-optic cable maps do not include information on the suitability of the fiber-optic cable for ground-motion sensing; fiber that is not coupled to the ground (e.g., strung between telephone poles or lying in a conduit) may not be suitable for ground-motion sensing. Although these deployment techniques are not common in metropolitan areas, more detailed fiber-optic cable maps from each ISP would be required to determine the suitability of each cable segment for ground-motion sensing.

Our study leveraged noise measurements from existing seismic sensors at a single frequency averaged over a single day to demonstrate the applicability of deploying new seismic sensors in fiber-optic cable to complement existing dedicated seismic sensors. This approach smoothed over diurnal variations of noise. In addition, many seismic sensors are tuned to measure a smaller band of frequencies, which may have been outside the range of this research's targeted frequency. This research describes a methodology to broadly understand the complementary opportunity that seismic sensing using existing ISP fiber-optic cable in metropolitan areas could provide. However, for specific use cases a more focused analysis must be conducted around the frequencies of interest, considering the variations in noise at existing and targeted sensors.

Conclusion

In this article, we assess the possible expansion of area monitored for ground motion if ISP fiber-optic cables were used for sensing. We found that the abundance of fiber-optic cable in metropolitan areas offers significant opportunity to extend the ground-motion event detection coverage area of the 100 most populous MSAs in the United States. Our method for conducting this analysis utilizes GIS to model layers of ground-motion detection coverage from existing point sensors and hypothetical fiber-based linearly distributed sensors inside the boundaries of metropolitan areas. Our analysis of the 100 most populous MSAs showed that, on an average, ISP fiber-optic cable used as ground-motion sensors could cover 18.7% of an MSA. Even when deployed in an optimal fashion to minimize costs, ISP fiber-optic cable used as sensors and existing seismic sensors could cover 12.2% of an MSA—an order of magnitude increase over what can be covered with existing seismic sensors. In two case studies of Little Rock, Arkansas, and Seattle, Washington, we showed that, even in MSAs with multiple seismic sensors, new sensors placed using fiber-optic cable could extend the ground-motion event detection area, which would provide exciting opportunities to monitor anthropogenic industrial, economic, and transportation activity in smart cities. Improved ground-motion detection in smart cities could be used to improve public safety, infrastructure management, emergency response, and our understanding of longer-term issues like anthropogenic responses to climate change.

Data and Resources

All data used in this article came from published sources listed in the references. In particular, information on existing seismic sensors in the United States may be obtained from IRIS Consortium (2023). Internet Atlas and United States long-haul infrastructure topology data, including fiber-optic shapefiles, may be requested from Impact Cyber Trust (2024).

Declaration of Competing Interests

The authors acknowledge that there are no conflicts of interest recorded.

Acknowledgments

This work is supported by the University of Wisconsin OVCRGE Research Forward program and National Science Foundation under Grant Numbers CNS-2106517, CNS-2312709, and CNS-2319367. Any opinions, findings, and conclusions or recommendations expressed in this material are those of the author(s) and do not necessarily reflect the views of the National Science Foundation.

References

Aazam, M., M. St-Hilaire, C.-H. Lung, and I. Lambadaris (2016). Cloud-based smart waste management for smart cities, *2016 IEEE 21st Int. Workshop on Computer Aided Modelling and Design of Communication Links and Networks (CAMAD)*, Toronto, Ontario, Canada, 23–25 October 2016, 188–193.

Adedeji, K. B., A. A. Ponnle, A. M. Abu-Mahfouz, and A. M. Kurien (2022). Towards digitalization of water supply systems for sustainable smart city development—Water 4.0, *Appl. Sci.* **12,** no. 18, 9174, doi: 10.3390/app12189174.

Ajo-Franklin, J. B., S. Dou, N. J. Lindsey, I. Monga, C. Tracy, M. Robertson, V. Rodriguez Tribaldos, C. Ulrich, B. Freifeld, T. Daley, *et al.* (2019). Distributed acoustic sensing using dark fiber for near-surface characterization and broadband seismic event detection, *Sci. Rep.* **9,** no. 1, 2045–2322.

Allen, R., P. Gasparini, O. Kamigaichi, and M. Bose (2009). The status of earthquake early warning around the world: An introductory overview, *Seismol. Res. Lett.* **80,** no. 5, 682–693.

Argany, M., M. Mostafavi, F. Karimipour, and C. Gagné (2011). A GIS based wireless sensor network coverage estimation and optimization: A Voronoi approach, in *Transactions on Computational Science XIV*, M. L. Gavrilova, C. J. K. Tan, and M. A. Mostafavi (Editors), Vol. 6970, Springer, Berlin, Heidelberg, doi: 10.1007/978-3-642-25249-5_6.

Cascone, V., J. Boaga, and G. Cassiani (2021). Small local earthquake detection using low-cost MEMS accelerometers: Examples in northern and central Italy, *Seism. Rec.* **1,** no. 1, 20–26.

Catudal, J., K. Dowsett, P. Barford, D. Fratta, B. Jensen, N. Lord, and H. Wang (2023). On the efficacy of using commodity optical transceivers for environmental sensing, *Opt. Fiber Sensors* doi: 10.1364/OFS.2023.W4.38.

Cunningham, E., N. Lord, D. Fratta, H. F. Wang, J. Catudal, and P. R. Barford (2022). Characterizing dark fiber das along a university campus route, *Eos. Trans. AGU*, Vol. **2022** (Fall Meet.), Abstracts S12D–0180.

D'Aniello, G., M. Gaeta, F. Orciuoli, G. Sansonetti, and F. Sorgente (2020). Knowledge-based smart city service system, *Electronics* **9,** no. 6, 965, doi: 10.3390/electronics9060965.

Diaz, J., M. Schimmel, M. Ruiz, and R. Carbonell (2020). Seismometers within cities: A tool to connect earth sciences and society, *Front. Earth Sci.* **8,** no. 9, doi: 10.3389/feart.2020.00009.

Dietel, C. (1995). Digital seismic recordings of the May 23, 1995, demolition of the Alfred P. Murrah federal building, Oklahoma City, Oklahoma, *U.S. Geol. Surv. Open-File Rept. 95-594*.

Durairajan, R., S. Ghosh, X. Tang, P. Barford, and B. Eriksson (2013). Internet atlas: A geographic database of the internet, *Proc. of the 5th ACM Workshop on HotPlanet*, New York, New York, Association for Computing Machinery, 15–20. 14

ESRI (2020). Esri ArcGIS, available at https://www.esri.com/. 15

Fu, J., Z. Li, H. Meng, J. Wang, and X. Shan (2019). Performance evaluation of low-cost seismic sensors for dense earthquake early warning: 2018–2019 field testing in southwest China, *Sensors* **19,** no. 9, 1999, doi: 10.3390/s19091999.

GeoPandas (2023). GeoPandas, available at https://geopandas.org/. 16

Impact Cyber Trust (2024). Impact cyber trust, available at https://www.impactcybertrust.org/. 17

Incorporated Research Institutions for Seismology (IRIS) Consortium (2023). IRIS Gmap, available at https://ds.iris.edu/gmap/. 18

Kenney, J. (1977). *Seismic Detection of Motor Vehicles*, Institute for Materials Research, U.S. Department of Transportation, Washington, D.C.

Kim, W., D. Simpson, and P. Richards (1994). High-frequency spectra of regional phases from earthquakes and chemical explosions, *Bull. Seismol. Soc. Am.* **84,** no. 5, 1365–1386.

Kirimtat, A., O. Krejcar, A. Kertesz, and M. Tasgetiren (2020). Future trends and current state of smart city concepts: A survey, *IEEE Access* **8,** 86,448–86,467.

Kong, Q., R. M. Allen, L. Schreier, and Y.-W. Kwon (2016). Myshake: A smartphone seismic network for earthquake early warning and beyond, *Sci. Adv.* **2,** no. 2, e1501055, doi: 10.1126/sciadv.1501055.

Krokidis, S., I. Vlachos, M. Avlonitis, A. Kostoglou, and V. Karakostas (2022). Data-driven performance evaluation of a low-cost seismograph, *Meas. Control.* **55,** nos. 5/6, 340–358.

Li, Z., Z. Shen, Y. Yang, E. Williams, X. Wang, and Z. Zhan (2021). Rapid response to the 2019 Ridgecrest earthquake with distributed acoustic sensing, *AGU Adv.* **2,** no. 2, e2021AV000395, doi: 10.1029/2021AV000395.

Liang, Z., N. Xu, K. Ma, S. Tang, and C. Tang (2013). Microseismic monitoring and numerical simulation of rock slope failure, *Int. J. Distrib. Sens. Netw.* **9,** no. 11, 845191.

Lindsey, N. J., E. R. Martin, D. S. Dreger, B. Freifeld, S. Cole, S. R. James, B. L. Biondi, and J. B. Ajo-Franklin (2017). Fiber-optic network observations of earthquake wavefields, *Geophys. Res. Lett.* **44,** no. 23, 11–792.

Lindsey, N. J., S. Yuan, A. Lellouch, L. Gualtieri, T. Lecocq, and B. Biondi (2020). City-scale dark fiber das measurements of infrastructure use during the covid-19 pandemic, *Geophys. Res. Lett.* **47,** no. 16, e2020GL089931, doi: 10.1029/2020GL089931.

Long, L. (1993). Measurements of seismic road vibrations, *International Conf. on Case Histories in Geotechnical Engineering*, Atlanta, Georgia, 3 June 1993, 6 pp.

Mahapatra, C., A. K. Moharana, and V. C. M. Leung (2017). Energy management in smart cities based on internet of things: Peak demand reduction and energy savings, *Sensors* **17,** no. 12, 2812, doi: 10.3390/s17122812.

Malekloo, A., E. Ozer, and F. Al-Turjman (2020). Combination of GIS and SHM in prognosis and diagnosis of bridges in earthquake-prone locations, in *Smart Grid in IoT-Enabled Spaces*, CRC Press. 19

Martin, E. R., C. M. Castillo, S. Cole, P. S. Sawasdee, S. Yuan, R. Clapp, M. Karrenbach, and B. L. Biondi (2017). Seismic monitoring leveraging existing telecom infrastructure at the SDASA: Active, passive, and ambient-noise analysis, *The Leading Edge* **36,** no. 12, 1025–1031.

20 Mendecki, A. (1996). *Seismic Monitoring in Mines*, Springer Science and Business Media.

Meng, H., Y. Ben-Zion, and C. Johnson (2021). Analysis of seismic signals generated by vehicle traffic with application to derivation of subsurface Q-values, *Seismol. Res. Lett.* **92,** no. 4, 2354–2363.

21 Missouri Department of Natural Resources (2023). Facts about the New Madrid Seismic Zone, available at https://dnr.mo.gov/land-geology/hazards/earthquakes/science/facts-new-madrid-seismic-zone.

Nirde, K., P. S. Mulay, and U. M. Chaskar (2017). IOT based solid waste management system for smart city, *2017 International Conf. on Intelligent Computing and Control Systems (ICICCS)*, Madurai, India, 15–16 June 2017, 666–669.

22 Optasense (2023). Distributed acoustic sensing interrogators, available at https://www.optasense.com/.

Parker, T., S. Shatalin, and M. Farhadiroushan (2014). Distributed acoustic sensing–A new tool for seismic applications, *First Break* **32,** no. 2, doi: 10.3997/1365-2397.2013034.

23 Patnaik, S., P. Barford, D. Fratta, B. Jensen, N. Lord, M. Malloy, and H. Wang (2021). Internet photonic sensing: Using internet fiber optics for vibration measurement and monitoring, *Proc. of the ACM SIGCOMM Workshop on Optical Systems (OptSys).*

Reilly, J., S. Dashti, M. Ervasti, J. D. Bray, S. D. Glaser, and A. M. Bayen (2013). Mobile phones as seismologic sensors: Automating data extraction for the Ishake system, *IEEE Trans. Autom. Sci. Eng.* **10,** no. 2, 242–251.

Rizwan, P., K. Suresh, and M. R. Babu (2016). Real-time smart traffic management system for smart cities by using internet of things and big data, *2016 International Conf. on Emerging Technological Trends (ICETT)*, Kollam, India, 21–22 October 2016, 1–7.

Schwardt, M., C. Pilger, P. Gaebler, P. Hupe, and L. Ceranna (2022). Natural and anthropogenic sources of seismic, hydroacoustic, and infrasonic waves: Waveforms and spectral characteristics (and their applicability for sensor calibration), *Surv. Geophys.* **43,** 1265–1361.

Shen, J., and T. Zhu (2021). Characterizing urban seismic noise recorded by distributed acoustic sensing array, *SEG International Exposition and Annual Meeting*, Denver, Colorado, 26 September–1 October 2021.

Shen, J., and T. Zhu (2021). Seismic noise recorded by telecommunication fiber optics reveals the impact of COVID-19 measures on human activity, *Seism. Rec.* **1,** no. 1, 46–55.

24 Silixa (2023). iDAS—Intelligent distributed acoustic sensor, available at https://www.silixa.com/.

Spica, Z., J. Ajo-Franklin, G. Beroza, B. Biondi, F. Cheng, B. Gaite, B. Luo, E. Martin, J. Shen, C. Thurber, *et al.* (2023). PubDAS: A public distributed acoustic sensing datasets repository for geosciences, *Seismol. Res. Lett.* **94,** no. 2A, 983–998.

25 U.S. Census Bureau (2023a). Cartographic boundary files—shapefiles, available at https://www.census.gov/geographies/mapping-files/time-series/geo/carto-boundary-file.html.

26 U.S. Census Bureau (2023b). Metropolitan and micropolitan statistical areas population totals and components of change: 2020-2021, available at https://www.census.gov/data/tables/time-series/demo/popest/2020s-total-metro-and_micro-statistical-areas.html.

27 U.S. Geological Survey (USGS) (2023). The New Madrid Seismic Zone, available at https://www.usgs.gov/programs/earthquake-hazards/new-madrid-seismic-zone.

28 U.S. Geological Survey (USGS) Earthquake Hazards Program (2023). Earthquake magnitude, energy release, and shaking intensity, available at https://www.usgs.gov/programs/earthquake-hazards/earthquake-magnitude-energy-release-and_shaking-intensity.

Vidale, J. E. (2011). Seattle “12th Man* Earthquake” goes viral, *Seismol. Res. Lett.* **82,** no. 3, 449–450.

Wang, H. F., X. Zeng, D. E. Miller, D. Fratta, K. L. Feigl, C. H. Thurber, and R. J. Mellors (2018). Ground motion response to an ml 4.3 earthquake using co-located distributed acoustic sensing and seismometer arrays, *Geophys. J. Int.* **213,** no. 3, 2020–2036.

Wang, X., E. Williams, M. Karrenbach, M. Herraez, H. Martins, and Z. Zhan (2020). Rose parade seismology: Signatures of floats and bands on optical fiber, *Seismol. Res. Lett.* **94,** no. 4, 2395–2398.

Wilson, D. C., E. Wolin, W. L. Yeck, R. E. Anthony, and A. T. Ringler (2021). Modeling seismic network detection thresholds using production picking algorithms, *Seismol. Res. Lett.* **93,** no. 1, 149–160.

Working Group on Instrumentation, Siting, Installation, and Site Metadata (2008). Instrumentation guidelines for the advanced national seismic system, *U.S. Geol. Surv. Open-File Rept. 2008–1262.*

Wuestefeld, A., and M. Wilks (2019). How to twist and turn a fiber: Performance modeling for optimal das acquisitions, *The Leading Edge* **38,** no. 3, 226–231.

Yin, J., W. Zhu, J. Li, E. Biondi, Y. Miao, Z. Spica, L. Viens, M. Shinohara, S. Ide, K. Mochizuki, *et al.* (2023). Earthquake magnitude with DAS: A transferable data-based scaling relation, *Geophys. Res. Lett.* **50,** no. 10, e2023GL103045, doi: 10.1029/2023GL103045.

Zhao, Y., E. Nilot, B. Li, G. Fang, W. Luo, and Y. Li (2023). Seismic attenuation extraction from traffic signals recorded by a single seismic station, *Geophys. Res. Lett.* **50,** no. 3, e2022GL100548, doi: 10.1029/2023GL103045.

Zhu, T., J. Shen, and E. R. Martin (2021). Sensing earth and environment dynamics by telecommunication fiber-optic sensors: an urban experiment in Pennsylvania, USA, *Solid Earth* **12,** no. 1, 219–235.

Appendix

Calculating detection threshold described our methodology to calculate detection thresholds from noise measurements. For

TABLE A1
Coefficients for Noise versus Distance for Equations (1)–(3) from Wilson *et al.* (2021)

Coefficient	*P*-Wave Value	Units
r_1	9.04×10^{1}	km
r_2	3.35×10^{2}	km
a_1	9.26×10^{-2}	M/km
a_2	−3.85	M/km
a_3	9.69×10^{-1}	M/km
b_1	1.03×10^{-2}	M/km
b_2	1.46×10^{-2}	M/dB
d	2.60×10^{-2}	M/dB
c	3.95	Magnitude (M)

Spatial analysis of the MSAs in the United States described in our analysis of the 100 most populous MSAs. Table A2 shows the ten largest MSAs by population.

TABLE A2
Largest Metropolitan Statistical Areas (MSAs) in the United States (by Population)

MSA Name	States	Population (millions)
New York–Newark–Jersey City	New York–New Jersey–Pennsylvania	20.3
Los Angeles–Long Beach–Anaheim	California	13.3
Chicago–Naperville–Elgin	Illinois–Indiana–Wisconsin	9.7
Dallas–Fort Worth–Arlington	Texas	7.5
Houston–The Woodlands–Sugar Land	Texas	7.0
Philadelphia–Camden–Wilmington	Pennsylvania–New Jersey–Delaware–Maryland	6.1
Washington–Arlington–Alexandria	District of Columbia–Virginia–Maryland–West Virginia	6.1
Miami–Fort Lauderdale–West Palm Beach	Florida	6.1
Atlanta–Sandy Springs–Roswell	Georgia	6.0
Boston–Cambridge–Newton	Massachusetts–New Hampshire	4.9

There are seven MSAs with ten or more active dedicated seismic sensors: Riverside–San Bernardino–Ontario, California (47 sensors); Portland–Vancouver–Hillsboro, Oregon–Washington (33 sensors); Seattle–Tacoma–Bellevue, Washington (27 sensors); Oklahoma City, Oklahoma (21 sensors); Tulsa, Oklahoma (17 sensors); Los Angeles–Long Beach–Anaheim, California (12 sensors); and Albuquerque, New Mexico (10 sensors).

TABLE A3
Comparison of Metropolitan Statistical Areas (MSA) Coverage Areas for the 75 Most Populous MSAs with Most Potential Total Detection Area (Including from Existing Seismic Sensors and Sensors Using Fiber-Optic Cable) for Low-Magnitude (M 0.5) Ground-Motion Events

MSA Name	States	MSA Area (km^2)	Existing Sensors Area (km^2)	All Fiber Area (km^2)	Fiber and Sensors Area (km^2)	Optimal Fiber and Sensors Area (km^2)
Dallas–Fort Worth–Arlington	Texas	23,332	2,713	8642	11,356	6828
Atlanta–Sandy Springs–Alpharetta	Georgia	22,899	0	8646	8646	5103
Minneapolis–St. Paul–Bloomington	Minnesota –Wisconsin	19,462	0	7243	7243	4123
Riverside–San Bernardino–Ontario	California	70,955	2496	3974	6470	4512
Chicago–Naperville–Elgin	Illinois–Indiana–Wisconsin	18,906	0	6461	6461	3997
New York–Newark–Jersey City	New York–New Jersey–Pennsylvania	19,048	6	6292	6298	3647
Philadelphia–Camden–Wilmington	Pennsylvania–New Jersey–Delaware–Maryland	12,285	0	6179	6179	3762
Pittsburgh	Pennsylvania	13,832	0	5800	5801	3197
Washington–Arlington–Alexandria	District of Columbia–Virginia–Maryland–West Virginia	17,429	0	5228	5228	3147
Houston–The Woodlands–Sugar Land	Texas	22,255	0	4497	4497	2312
Charlotte–Concord–Gastonia	North Carolina–South Carolina	14,787	0	4303	4303	2599
Las Vegas–Henderson–Paradise	Nevada	20,880	2739	1537	4276	3522
Detroit–Warren–Dearborn	Michigan	10,415	0	4231	4231	2511
Miami–Fort Lauderdale–Pompano Beach	Florida	14,159	0	4168	4168	2656

(Continued next page.)

TABLE A3 (continued)

Comparison of Metropolitan Statistical Areas (MSA) Coverage Areas for the 75 Most Populous MSAs with Most Potential Total Detection Area (Including from Existing Seismic Sensors and Sensors Using Fiber-Optic Cable) for Low-Magnitude (M 0.5) Ground-Motion Events

MSA Name	States	MSA Area (km²)	Existing Sensors Area (km²)	All Fiber Area (km²)	Fiber and Sensors Area (km²)	Optimal Fiber and Sensors Area (km²)
Seattle–Tacoma–Bellevue	Washington	15,535	1006	3046	4052	2868
Indianapolis–Carmel–Anderson	Indiana	11,235	0	3927	3927	2445
Albuquerque	New Mexico	24,068	2818	1003	3821	3150
Phoenix–Mesa–Chandler	Arizona	37,797	0	3474	3474	2234
Denver–Aurora–Lakewood	Colorado	21,746	463	3007	3470	2268
Los Angeles–Long Beach–Anaheim	California	12,677	141	3321	3462	1905
Cleveland–Elyria	Ohio	5215	0	3446	3446	2081
Omaha–Council Bluffs	Nebraska–Iowa	11,423	0	3404	3404	2013
Ogden–Clearfield	Utah	22,357	2752	651	3403	3177
Des Moines–West Des Moines	Iowa	9434	0	3385	3385	2085
Salt Lake City	Utah	20,961	2033	1319	3352	2831
Kansas City	Missouri–Kansas	19,089	0	3294	3294	2039
Columbus	Ohio	12,560	0	3271	3271	1957
Little Rock–North Little Rock–Conway	Arkansas	10,868	704	2555	3259	2107
Nashville–Davidson–Murfreesboro–Franklin	Tennessee	14,922	0	3154	3154	1844
St. Louis	Missouri–Illinois	20,944	0	2598	2598	1826
Cincinnati	Ohio–Kentucky–Indiana	11,999	0	2508	2508	1635
Richmond	Virginia	11,629	0	2442	2442	1480
Memphis	Tennessee–Mississippi–Arkansas	12,163	0	2436	2436	1463
Louisville/Jefferson County	Kentucky–Indiana	8521	50	2330	2380	1377
Birmingham–Hoover	Alabama	11,813	209	2143	2352	1428
San Francisco–Oakland–Berkeley	California	6627	8	2322	2330	1254
Tulsa	Oklahoma	16,745	1	2264	2264	1358
Virginia Beach–Norfolk–Newport News	Virginia–North Carolina	9783	0	2204	2204	1224
San Diego–Chula Vista–Carlsbad	California	11,019	1175	905	2080	1839
Toledo	Ohio	4248	0	1870	1870	1060
Jacksonville	Florida	8866	0	1819	1819	1061
Portland–Vancouver–Hillsboro	Oregon–Washington	17,662	229	1554	1783	1176
Oklahoma City	Oklahoma	14,452	0	1747	1747	1209
Baltimore–Columbia–Towson	Maryland	7015	0	1730	1730	887
San Antonio–New Braunfels	Texas	19,076	7	1681	1688	1015
Tampa–St. Petersburg–Clearwater	Florida	6936	0	1655	1655	1029

(Continued next page.)

TABLE A3 (continued)

Comparison of Metropolitan Statistical Areas (MSA) Coverage Areas for the 75 Most Populous MSAs with Most Potential Total Detection Area (Including from Existing Seismic Sensors and Sensors Using Fiber-Optic Cable) for Low-Magnitude (M 0.5) Ground-Motion Events

MSA Name	States	MSA Area (km^2)	Existing Sensors Area (km^2)	All Fiber Area (km^2)	Fiber and Sensors Area (km^2)	Optimal Fiber and Sensors Area (km^2)
Deltona–Daytona Beach–Ormond Beach	Florida	4590	0	1532	1532	1017
Provo–Orem	Utah	14,366	825	648	1472	1038
Winston–Salem	North Carolina	5281	0	1458	1458	861
Austin–Round Rock–Georgetown	Texas	11,075	0	1415	1415	880
Madison	Wisconsin	8773	1	1395	1396	975
Grand Rapids–Kentwood	Michigan	7119	0	1383	1383	888
Milwaukee–Waukesha	Wisconsin	3866	0	1344	1344	800
Spokane–Spokane Valley	Washington	11,184	802	531	1333	1124
Akron	Ohio	2392	0	1333	1333	778
El Paso	Texas	14,460	239	1090	1329	850
Sacramento–Roseville–Folsom	California	13,743	30	1285	1315	779
Boston–Cambridge–Newton	Massachusetts–New Hampshire	9501	7	1302	1309	937
Wichita	Kansas	10,828	0	1257	1257	741
Harrisburg–Carlisle	Pennsylvania	4310	8	1234	1242	692
Orlando–Kissimmee–Sanford	Florida	10,381	0	1226	1226	756
Greenville–Anderson	South Carolina	7216	0	1220	1220	442
Worcester	Massachusetts–Connecticut	5443	3	1204	1207	717
Syracuse	New York	6433	1	1176	1177	676
Allentown–Bethlehem–Easton	Pennsylvania–New Jersey	3818	0	1144	1144	677
Columbia	South Carolina	9922	2	1080	1081	641
Tucson	Arizona	23,790	235	842	1077	720
Augusta–Richmond County	Georgia–South Carolina	9273	0	1056	1056	573
Cape Coral–Fort Myers	Florida	2299	0	1026	1026	668
Scranton–Wilkes-Barre	Pennsylvania	4598	0	1018	1018	548
Knoxville	Tennessee	8677	6	939	946	593
Dayton–Kettering	Ohio	3344	0	891	891	507
Boise City	Idaho	30,629	0	873	873	564
Albany–Schenectady–Troy	New York	7450	0	848	848	483
San Jose–Sunnyvale–Santa Clara	California	6967	33	784	817	473

reference, we reproduced the coefficients for equations (1)–(3) for P waves calculated by Wilson *et al.* (2021) in Table A1. 29

Manuscript received 31 January 2024

Queries

1. AU: The citation "Shen *et al.*, 2021" does not have a corresponding Reference entry. There is a "Shen and Zhu 2021" in the References, which is not cited in the paper. Please (1) decide whether these refer to the same work and (2) indicate the required changes to the paper and the References.
2. AU: SSA reserves "while" to describe events that happen simultaneously. When this is not the case, "while" has been changed to "although" or "whereas" throughout. Please provide revisions if necessary.
3. AU: SSA uses "because" instead of "since" or "as" unless they are intended to refer to time or specific mathematical conditions. Would it be consistent with your meaning here to change "as" to "because"?
4. AU: Please indicate if the roman capital M throughout the article should be changed to (1) bold **M** or (2) *M*_w (italic "M" and subscript roman "w").
5. AU: Please confirm whether the edited changes to the Sentence "Technology use often includes" does not affect your intended meaning.
6. AU: As per SSA style, the abbreviation "(ANSS)" has been deleted because it is not used again in this article.
7. AU: As per SSA style, the abbreviation "(ANSS)" has been deleted because it is not used again in this article.
8. AU: Please confirm the edited changes to the Sentence "Argany *et al.* (2011) present a survey of techniques…" does not affect your intended meaning.
9. AU: There are two U.S. Census Bureau (2023) references in the reference section (now denoted as 2023a and 2023b). Please specify which is being cited here.
10. AU: As per SSA style, the abbreviation "(PoP)" has been deleted because it is not used again in this article.
11. AU: As per SSA style, the abbreviation "(GSN)" has been deleted because it is not used again in this article.
12. AU: Per style, Tables 4, 5, and 6 have been modified to Tables A1, A2, and A3. Kindly confirm whether the edited changes does not affect your intended meaning.
13. AU: Please specify what does "KDK" indicates.
14. AU: For Durairajan et al. (2013) please provide the days, month, and year when the conference was held.
15. AU: For ESRI (2020) please provide the month and year when you last accessed the website.
16. AU: For GeoPandas (2023) please provide the month and year when you last accessed the website.
17. AU: For Impact Cyber Trust (2024) please provide the month and year when you last accessed the website.
18. AU: For IRIS Consortium (2023) please provide the month and year when you last accessed the website.
19. AU: For reference Malekloo et al. (2020) Please provide editor name(s) and location of publisher.
20. AU: For reference Mendecki (1996) Please provide location of publisher.
21. AU: For Missouri Department of Natural Resources (2023) please provide the month and year when you last accessed the website for your article.
22. AU: For Optasense (2023) please provide the month and year when you last accessed the website for your article.
23. AU: For Patnaik et al. (2021) Please provide the Conference date with the location where was held.
24. AU: For Silixa (2023) please provide the month and year when you last accessed the website for your article.
25. AU: For U.S. Census Bureau (2023a) please provide the month and year when you last accessed the website for your article.
26. AU: For United States Census Bureau (2023b) please provide the month and year when you last accessed the website for your article.
27. AU: For U.S. Geological Survey (USGS) (2023) please provide the month and year when you last accessed the website for your article.
28. AU: For U.S. Geological Survey (USGS) Earthquake Hazards Program (2023) please provide the month and year when you last accessed the website for your article.
29. AU: Please note that as per SSA style, Appendix section must contain an introductory text and all the appendix elements (figures and tables) should be cross referred in that introductory text. So, kindly cite Appendix Tables A2 and A3 in Appendix section.
30. AU: Please note that figure legends and axis labels are edited to match the SSA style and to be consistent with the text. Please verify the changes and confirm whether the changes do not affect your intended meaning.
31. AU: The set up of Tables 1 to 3 and A1 to A3 have been changed to conform with SSA style. Please check that your meaning was retained.